



Dehydration of supercritical carbon dioxide using dense polymeric membranes: A techno-economical evaluation



Andrew Shamu^{a,b}, Henk Miedema^a, Zandrie Borneman^{b,c}, Kitty Nijmeijer^{b,c,*}

^a Wetsus, Centre of Excellence for Sustainable Water Technology, Oostergoweg 9, 8911 MA Leeuwarden, the Netherlands

^b Membrane Materials and Processes, Eindhoven University of Technology, P.O. Box 513, 5600 MB Eindhoven, the Netherlands

^c Dutch Institute for Fundamental Energy Research (DIFFER), P.O. Box 6336, 5600 HH Eindhoven, the Netherlands

ARTICLE INFO

Keywords:

Supercritical fluids
Carbon dioxide
Gas separation
Membranes
Food drying
Process modeling

ABSTRACT

Supercritical CO₂ (scCO₂), used in the food industry as a water extraction agent, requires dehydration units for regeneration. The present study assesses the economics of membrane-based dehydration of scCO₂. In contrast to earlier studies, the contribution, next to the membrane, also the contributions of the mass transfer resistances of the feed and permeate boundary are included, which have a dominant effect on the final process design and economics. In addition, our work also extrapolates the process to industrial scale evaluating different configurations and process conditions. Specifically, the contribution of the membrane and membrane unit costs is discussed in more detail. Including the mass transfer resistances of feed and permeate boundary layer reduces the water flux across the membrane up to a factor 150, implying a larger required membrane surface area for a given water removal rate, and thus higher costs. Using a SPEEK-based membrane, the total drying costs, normalized for the amount of water removed, minimize around a skin layer thickness of 1 μm, i.e., not too thin to permeate and thus spill too much CO₂ and not too thick to hamper the H₂O flux. Because the feed boundary layer dominates water transport, conditions that minimize its thickness reduce total costs. A reduction of the feed boundary layer dominance can be achieved by adjusting channel height, cross-flow velocity and the density and viscosity of scCO₂, the latter two by increasing the operational temperature from 45 to 65 °C (at 130 bar). Compared to the benchmark zeolite process currently available, the membrane-based process for drying scCO₂ outlined and optimized in the present study results in a 50% saving of total drying costs. These savings can be achieved by using a dense polymeric membrane with a H₂O permeability of at least 10,000 Barrer and a CO₂ permeability of at most 10 Barrer.

1. Introduction

Supercritical carbon dioxide (scCO₂) is an inexpensive and therefore attractive solvent for the dehydration of food products because it combines non-toxicity with a near-ambient critical temperature, preventing thermal denaturation and a moderate critical pressure [1]. During supercritical dehydration, the product does not experience any capillary stresses due to the absence of clear liquid-vapor interfaces. In conventional evaporation processes, these interfaces cause shrinkage and structural damages of the product [2]. This defines scCO₂-based dehydration as a very gentle process able to preserve the texture of the food [3]. After food dehydration, scCO₂ is easily separated from the food product through depressurization, resulting in the discharge of gaseous CO₂. Depressurization is also used to regenerate, i.e., dehydrate, scCO₂, by making use of the fact that the solubility of H₂O in

scCO₂ shows a minimum near the critical pressure of 74 bar [4,5]. However, this regeneration method is rather energy-consuming due to the necessity to repressurize CO₂ afterwards to its extraction pressure. More energy efficient is the adsorption-based regeneration using zeolite [6], displayed in Fig. 1. Here, humid scCO₂, leaving the fruit extraction unit, is regenerated in the dehydration unit before its next re-injection into the extraction unit. The zeolite, located in the dehydration unit, adsorbs water up to its saturation level. The re-use of zeolite demands an energy-intensive reactivation step using hot air to desorb the water. A second, parallel regeneration unit ensures continuity of the scCO₂ dehydration process. Common fluid pressures and temperatures of the food drying process are 130 bar and 45 °C, thus above the critical point of CO₂ (T_c = 31.04 °C, P_c = 73.8 bar) [7].

Even though the zeolite-based regeneration of scCO₂ is energy-wise more efficient than the depressurization of scCO₂, the method still is

* Corresponding author at: Membrane Materials and Processes, Eindhoven University of Technology, P.O. Box 513, 5600 MB Eindhoven, the Netherlands.
E-mail address: d.c.nijmeijer@tue.nl (K. Nijmeijer).

<https://doi.org/10.1016/j.seppur.2019.05.027>

Received 5 February 2019; Received in revised form 7 May 2019; Accepted 7 May 2019

Available online 08 May 2019

1383-5866/ © 2019 The Authors. Published by Elsevier B.V. This is an open access article under the CC BY-NC-ND license (<http://creativecommons.org/licenses/by-nc-nd/4.0/>).

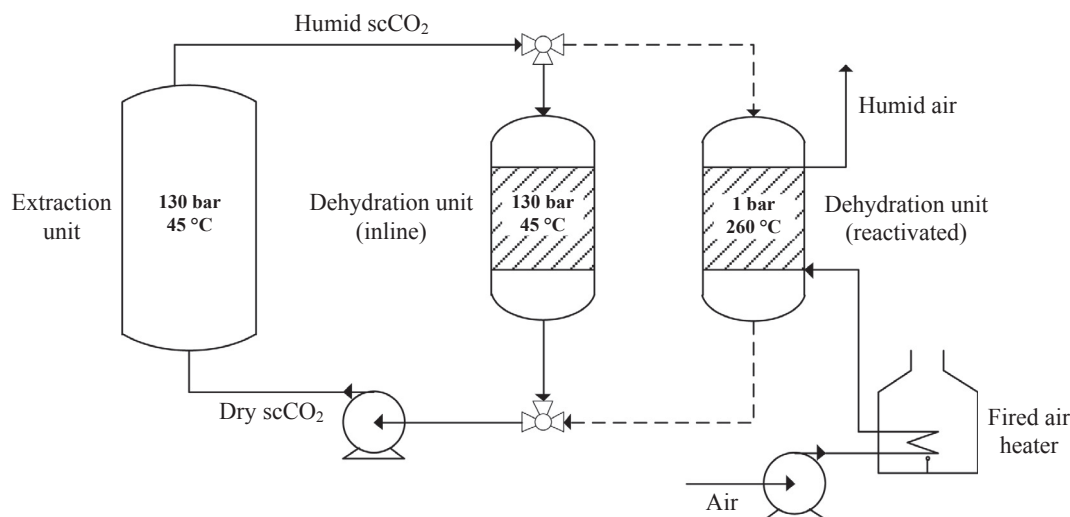


Fig. 1. Schematic depiction of a food dehydration process using scCO_2 as the water-extraction agent (left unit) and zeolite to dehydrate (regenerate) scCO_2 . A second dehydration unit is in stand-by mode and enables continuity of the entire process.

rather energy-intensive. Lohaus et al. [8] showed that membrane-based dehydration of scCO_2 can reduce the dehydration costs up to 20%. However, their conclusion was based on pilot plant-scaled processes having scCO_2 flow rates of 200 kg/h, corresponding to a water removal rate of only 0.32 kg/h. Moreover, their analysis omitted considering the individual mass transfer resistances related to the membrane skin layer and its support as well as the feed and permeate boundary layer. Oppositely, in a recent publication, we did identify a distinct contribution of each of these mass transfer resistances though [9]. Whereas the feed boundary layer comprises up to 80% of the overall mass transport resistance of H_2O , the dominant resistance for CO_2 is located within the membrane itself, leading to different conclusions. Inspired by Lohaus et al. [8], the present study reassesses the economics of membrane-based dehydration of scCO_2 , including the contribution of individual mass transfer resistances and thereby extrapolating the process to industrial scale and evaluating configuration and process conditions. Also, in particular the contribution of membrane and membrane unit costs is discussed in more detail.

2. Techno-economic process description

2.1. Extraction unit

The starting point of the simulations is the extraction unit, displayed in Fig. 1. The determination of the water-removal rate of the process requires knowledge of the mass of food product, its initial and final moisture content and the dehydration time. Following Kaymak-Ertekin et al. [10] the initial and final moisture content is set to 82 wt% and 12 wt%, respectively, the latter representing the average of the moisture content of dried fruits (17 wt%) and vegetables (7 wt%) [11].

The water removal rate during one extraction cycle $\dot{m}_{\text{H}_2\text{O}}$ is defined by:

$$\dot{m}_{\text{H}_2\text{O}} = \frac{m_{\text{food}}}{t_{\text{cycle}}} \cdot \frac{M_{\text{H}_2\text{O},\text{in}} - M_{\text{H}_2\text{O},\text{out}}}{M_{\text{H}_2\text{O},\text{in}} + 1} \quad (1)$$

where m_{food} is the mass of undried food (kg), $M_{\text{H}_2\text{O},\text{in}}$ and $M_{\text{H}_2\text{O},\text{out}}$ are the initial and final moisture contents of the food given in ($\text{kg}_{\text{H}_2\text{O}}/\text{kg}_{\text{drymass}}$), respectively and t_{cycle} is the duration of one food drying cycle.

The mass flow rate of scCO_2 needed for extraction \dot{m}_{scCO_2} , is described by:

$$\dot{m}_{\text{scCO}_2} = \frac{\dot{m}_{\text{H}_2\text{O}}}{w_{\text{H}_2\text{O},\text{out}} - w_{\text{H}_2\text{O},\text{in}}} \quad (2)$$

where $w_{\text{H}_2\text{O},\text{in}}$ and $w_{\text{H}_2\text{O},\text{out}}$ are the H_2O weight fractions of scCO_2 entering and exiting the extraction unit (–), respectively. For both, the zeolite and the membrane-based process, the latter stream is considered saturated, implying that its H_2O weight fraction is determined with the model developed by Spycher et al. [5]. The H_2O weight fraction of the scCO_2 stream entering the extraction unit differs for both processes. For the zeolite-based process, all the water dissolved in scCO_2 is considered to be fully adsorbed in the dehydration unit, indicating a completely dry regenerated stream. For the membrane-based process, a full water removal would require infinite membrane area, which is not possible. Therefore, a minimal amount of water will stay present in the regenerated stream. Its concentration, being low enough to still enable food dehydration down to its final moisture content, is determined using the GAB model [10], as discussed in Section 2.2.

The volume of the extraction unit is determined using the mass of the fresh food and its bulk density (500 kg/m^3). To include distribution equipment and free space into account as well, the total volume is multiplied by a factor of 1.2 [12].

The duration of one food drying cycle 4 hrs. This is slightly longer than the drying time of 2.5 h measured at lab-scale by Brown et al. [3], but necessary to avoid extensive shear stresses which the product is exposed to due to increased scCO_2 velocities in the extraction chamber. This happens when scaling up from lab-scale to industrial scale while maintaining the retention time of the scCO_2 in the extraction chamber.

2.2. Membrane-based process

Fig. 2 displays the default configuration of the membrane-based process, where the temperature and pressure of the feed cycle, thus in the extraction and membrane unit, are maintained at 45°C and 130 bar.

During the dehydration process, humid supercritical CO_2 enters the feed channel of the membrane unit, is dehydrated and exits as a dry scCO_2 stream ready for reuse as a drying agent. Pre-dried and heated CO_2 at ambient pressures is used as a sweep gas to maintain a high driving force by removing water vapor at the permeate side of the membrane unit. The usage of pre-dried air instead as a sweep gas is strictly avoided, even though its usage might be more cost effective, due to air permeation into the feed, thus impurification of the feed cycle. During the drying process, CO_2 permeates as well. To prevent any accumulation in the permeate cycle CO_2 is re-injected into the feed cycle using a refill pump.

Based on the previous work [9], the membrane-based dehydration unit has a flat sheet membrane configuration (Fig. 3).

Multiple, parallelly arranged composite membranes, having a

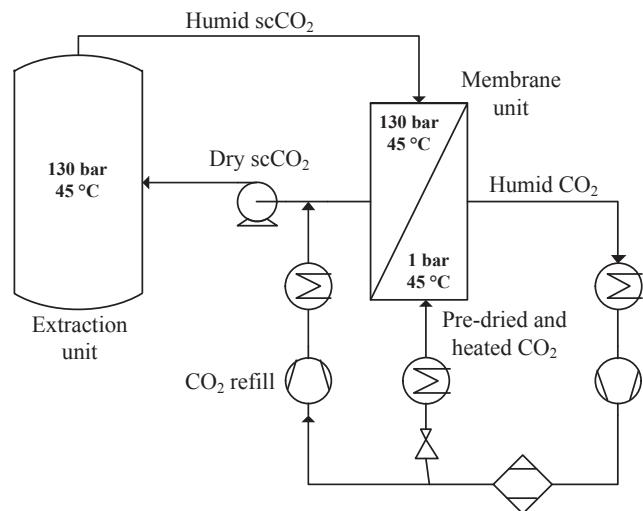


Fig. 2. The membrane-based process for the dehydration of scCO₂. The temperature and pressure of the humid scCO₂ are not changed before entering the membrane unit. CO₂ is cyclically used as a sweep gas to remove the permeated water from the membrane unit.

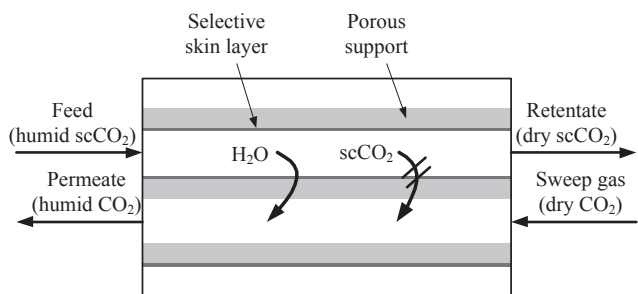


Fig. 3. Schematic depiction of the flat sheet membrane design considered in previous studies [9]. A gradual decay of the water content within the feed stream is caused by a selective water permeation through the skin layer. ScCO₂ is rejected and exits the membrane unit as a dry stream ready for reuse as an extraction agent.

selective skin layer on top of a porous support, are compiled into one membrane stack. These flat sheets are separated by feed and permeate channels having heights of 0.8 mm and 3 mm, respectively. The latter channel is chosen narrower than 7 mm as used in previous studies [9] to increase the compactness of the membrane unit, thus to reduce its scale and the investment costs associated with it.

Table 1 lists the geometric characteristics of the evaluated composite membrane based on specifications of commercially available composite membranes [13].

As in the previous study [9], three different selective layer membrane materials are evaluated: highly water permeable and H₂O/CO₂ selective SPEEK, Nafion® 117 and PEBAX® 1074. Especially SPEEK proved to withstand months-long exposure to corrosive flue gas streams [14]. The intrinsic, mixed gas H₂O permeabilities and pure gas CO₂ permeabilities, measured at 30 °C and near atmospheric pressures [13,14], were chosen as model input (Table 2), due to the absence of corresponding permeabilities within the supercritical region.

Table 1
Properties of the composite membrane used for the simulations.

Property	Porous support	Selective skin layer
Pore size	0.1 μm	Dense, non-porous polymer
Porosity	0.7	
Thickness	120 μm	1 μm

These permeabilities probably do not reflect the skin layer permeability at supercritical conditions. To assess the effect of this, a sensitivity analysis of the H₂O and CO₂ permeability on the outcomes is performed.

To determine the H₂O and CO₂ flux (permeability is a membrane characteristic independent of the actual process conditions) through the membrane, the corresponding driving forces are required. The H₂O driving force equals the logarithmic mean fugacity difference of the feed, retentate, permeate and sweep gas:

$$\Delta f_{H_2O} = \frac{(f_{in,H_2O}^F - f_{out,H_2O}^P) - (f_{out,H_2O}^F - f_{in,H_2O}^P)}{\ln \frac{f_{in,H_2O}^F - f_{out,H_2O}^P}{f_{out,H_2O}^F - f_{in,H_2O}^P}} \quad (3)$$

where Δf_{H_2O} is the H₂O driving force, f_{in,H_2O}^F and f_{out,H_2O}^F are the fugacities of H₂O in the feed and retentate stream and f_{in,H_2O}^P and f_{out,H_2O}^P are the fugacities of H₂O in the sweep gas and permeate stream (Pa), respectively. Since CO₂ fugacity of the permeate side is negligibly small compared to that of the feed and retentate stream, the CO₂ driving force equals the CO₂ fugacity difference between feed- and permeate stream.

The required H₂O and CO₂ fugacities are determined using,

$$f_i = \phi_i \cdot y_i \cdot P_{tot} \quad (4)$$

where ϕ_i and y_i are the dimensionless fugacity coefficient and mole fraction of component i in the fluid phase, respectively. P_{tot} is the total fluid pressure (Pa). The CO₂ fugacity coefficient is determined using the model of Spycher et al. [5] whereas the former model and the Antoine equation [15] are used to determine the fugacity coefficient and mole fraction of H₂O at saturation for supercritical and ambient conditions, respectively.

For non-saturated streams, the actual H₂O fugacity is lower than the corresponding H₂O fugacity at saturation, being determined by the model of Spycher et al. [5] and the Antoine equation [15]. Therefore, the H₂O fugacity at saturation of equation (4), is reduced by the water activity of the non-saturated stream as shown by:

$$f_{H_2O} = a_w \cdot f_{H_2O,sat} \quad (5)$$

where f_{H_2O} and $f_{H_2O,sat}$ are the required H₂O fugacity and H₂O fugacity at saturation (Pa), respectively and a_w is the water activity being dimensionless.

The water activity of the feed stream entering the membrane unit is fully saturated ($a_w = 1$). The water activity of the retentate stream, leaving the membrane unit is dependent on the final moisture content of the food product (12 wt%) and is determined using the Guggenheim–Andersen–de Boer (GAB) model [10]. This model links the equilibrium moisture content of food products to the water activity of the surrounding fluid at atmospheric pressures:

$$M = \frac{M_0 \cdot C \cdot K \cdot a_w}{[(1 - K \cdot a_w)(1 - K \cdot a_w + C \cdot K \cdot a_w)]} \quad (6)$$

where M_0 is the monolayer moisture content given in ($kg_{H_2O}/kg_{drymass}$), C and K are dimensionless empirical GAB parameters and a_w is the water activity (–). Assuming pressure insensitivity of the H₂O fugacity on the equilibrium moisture content of food products, the model can be extended to supercritical pressures. By doing so, the water activity of the retentate stream equals 0.25, considering an equilibrium moisture content of 12 wt% of the food product at 45 °C and 130 bar. The water fugacity of the retentate is determined with equation (5). Here the calculated water activity and the water fugacity of saturated air at the corresponding temperature at atmospheric pressures are used.

The weight fraction of H₂O in the retentate stream needed for equation (2) is derived from its corresponding molar fraction which is determined by rearranging equation (4).

Before entering the permeate side, the sweep gas is pre-dried using a refrigeration dryer, which uses the water solubility lowering effect of gas compression and cooling for gas drying. Cooling down the sweep

Table 2

H₂O and CO₂ permeability of SPEEK, Nafion® 117 and PEBAX® 1074 membranes. Data for SPEEK have been obtained from [14] (CO₂) and [15] (H₂O), data for Nafion® 117 from [16] (CO₂) and [17] (H₂O) and for PEBAX® 1074 from [14].

Polymer	Abbreviation	H ₂ O permeability (Barrer)	CO ₂ permeability (Barrer)
Sulfonated polyetheretherketon	SPEEK	61,000	0.11
Perfluorosulfonic acid/Polytetrafluoroethylene copolymer	Nafion® 117	410,000	2.8
Poly(amide-12-b-ethylene oxide)	PEBAX® 1074	200,000	122

gas to +3 °C (a typical temperature for refrigeration dryers [18]), while compressing it to 3 bar results in a dew point temperature of −11.6 °C. Using the Antoine equation [15], the water activity of the pre-dried sweep gas entering the membrane unit is 0.026 at 45 °C. For the exiting humidified sweep gas stream a water activity of 0.45 is considered, which is high enough to enable water removal with a moderate sweep gas volume flow rate while being low enough to maintain a sufficient driving force for the H₂O transport.

To withstand high pressures, the membrane unit is considered to be a cylindrically shaped pressure vessel containing a stack of flat sheets. This stack is square-shaped whereas its diagonal is considered to be equal to the vessels diameter. An increase in the considered vessel diameter results therefore in increased stack height and width thus to a larger membrane sheet (due to increased stack height) and a larger number of flat sheets placed within the stack (due to increased stack width), when keeping the feed and permeate channel heights constant. Knowing the volume flow rate of the feed and permeate streams and the number of feed and permeate channels including their cross-sectional areas, one can determine the channels fluid velocities and the mass transfer resistances in the channels. This together with the mass transfer properties of the composite membrane results in an overall mass transfer coefficient for H₂O and CO₂, which describes their transport from feed to permeate side. Previous work [9] gives a detailed description of the overall mass transfer coefficient determination and we follow a similar approach.

Together with the water transport driving force the required membrane area for the dehydration of humid scCO₂ can now be determined:

$$A = \frac{\dot{m}_{H_2O} \cdot R \cdot T}{M_{H_2O} \cdot k_{ov,H_2O} \cdot \Delta f_{H_2O}} \quad (7)$$

where \dot{m}_{H_2O} is the permeated mass flow rate of water (kg/s), R the ideal gas constant (J/(mol·K)), T the dehydration temperature in the membrane unit (K), M_{H_2O} is the molar mass of water (kg/mol), k_{ov,H_2O} the overall mass transfer coefficient (m/s) and Δf_{H_2O} the process driving force (Pa).

The volume flow rate of the sweep gas stream (\dot{V}_{sweep}), given in m³/s, is determined by:

$$\dot{V}_{sweep} = \frac{\dot{m}_{H_2O} \cdot R \cdot T}{M_{H_2O} \cdot (f_{out,H_2O}^p - f_{in,H_2O}^p)} \quad (8)$$

Using the membrane area and the number and thickness of the membrane sheets, the length of the stack equals:

$$L = \frac{A}{N_{sheet} \cdot \hat{A} \cdot h_{sheet}} \quad (9)$$

where N_{sheet} is the number of membrane sheets (–) and h_{sheet} is the height of one flat sheet membrane including spacer and channel height (m). The vessel of the membrane unit is considered 1.2 times longer than the calculated membrane stack height to ensure enough space for equipment, distributing the feed and sweep gas streams into its corresponding channels and collecting these streams afterwards [12].

The membrane unit length is therefore indirectly a function of its diameter. As in the previous study [9], its length is limited by the maximally allowed pressure drop of 1.5 bar and 50 mbar in the feed and permeate channel, respectively. The pressure drop ΔP , given in Pa, is

determined using [19]:

$$\Delta P = 4 \cdot f \cdot \frac{l}{d_h} \cdot \frac{\rho \cdot v^2}{2} \quad (10)$$

where f is the Fanning friction factor (–), l is the length of the membrane (m), ρ is the fluid density (kg/m³), v is the fluid velocity in the feed/permeate channel (m/s), d_h is the hydraulic diameter (m) which is for rectangular channels with much greater width than height, twice the height. At laminar conditions, the Fanning friction factor is the quotient of 14.227 and the Reynolds number, whereas for turbulent conditions the following relation is used [19],

$$f = \frac{1}{\left(-4 \cdot \log\left(\frac{0.27 \cdot \varepsilon}{d_h} + \left(\frac{7}{Re}\right)^{0.9}\right)\right)^2} \quad (11)$$

where ε is the surface roughness coefficient of the channel walls, which is assumed similar to the value of polyvinyl chloride (2.1·10^{−6} m) [20].

Now after determining the final dimensions of the membrane unit, the mass of permeated CO₂ can be determined. For this, the overall mass transfer coefficient of CO₂, its driving force and the membrane area are implemented into the rearranged equation (7).

2.3. Zeolite-based process

The mass of zeolite needed for adsorption ($m_{zeol.}$) is determined by:

$$m_{zeol.} = \frac{m_{H_2O}}{(X_{45^\circ C} - X_{260^\circ C})} \quad (12)$$

where m_{H_2O} is the amount of adsorbed water per drying cycle (kg), $X_{45^\circ C}$ and $X_{260^\circ C}$ are the zeolite water adsorption capacities being 0.20 and 0.02 kg_{H₂O}/kg_{zeolite}, respectively [21]. Previous adsorption capacities, determined at near atmospheric pressures, were considered due to the absence of high pressure adsorption capacities. The zeolite mass, $m_{zeol.}$ is used together with the zeolite bulk density, 728.8 kg/m³ [22], to determine the volume and dimensions of the dehydration vessel. Likewise to the extraction unit, the total volume is multiplied by 1.2 to account for additional vessel height due to implemented distribution equipment, required for an uniform dispersion of the humid scCO₂ in the adsorption column.

Lohaus et al. [8] considered 3.3 kWh as the total energy demand needed to remove 1 kg of water from zeolite. This mass-specific energy includes desorption and heating of the zeolite and its periphery (i.e., adsorption column). The product of this mass-specific energy demand and the adsorbed water mass per drying cycle equals the thermal energy needed for zeolite reactivation, being provided by hot air, which mass (m_{air}) is:

$$m_{air} = \frac{E_{reac.}}{c_{p,air} \cdot \hat{A} \cdot (T_{zeol.in} - T_{zeol.out})} \quad (13)$$

where $E_{reac.}$ is the required thermal energy (kJ), $c_{p,air}$ is the isobaric heat capacity of air (kJ/(kg·K)), $T_{zeol., in}$ and $T_{zeol., out}$ are the temperatures of the air entering and exiting the zeolite column (K) and m_{air} is the required mass of air needed for reactivation (kg). The latter is used to determine the heat duty of the fired air heater:

$$W_{heat} = \frac{m_{air} \cdot c_{p,air} \cdot \hat{A} \cdot (T_{air,out} - T_{air,in})}{t_{reac.}} \quad (14)$$

Table 3
Required parameters for the determination of the heat duty of the fired heater.

Parameter	Value	Reference
Inlet air temperature of the reactivated zeolite column ($T_{zeol, in}$)	260 °C	[23]
Outlet air temperature of the reactivated zeolite column ($T_{zeol, out}$)	175 °C	[23]
Inlet air temperature of the direct-fired heater ($T_{air, in}$)	20 °C	[est. ^a]
Outlet air temperature of the direct-fired heater ($T_{air, out}$)	260 °C	[23]
The isobaric heat capacity of air ($c_{p, air}$)	1.04 kJ/(kg·K)	[19]
Reactivation time per zeolite column (t_{reac})	1.5 h	[est.]
Time for the mounting and down-cooling of the reactivated zeolite column	0.5 h	[est.]
Adsorption time	2 h	[est.]
Energy demand for reactivation of Zeolite (E_{reac})	11,880 kJ/kg _{H₂O}	[8]

^a est. = estimated.

where $T_{air, in}$ and $T_{air, out}$ are the temperatures of the in- and outlet of the direct-fired heater (K), t_{reac} is the time considered for the reactivation (s) and W_{heat} is the thermal performance of the direct-fired heater (kW).

All parameters needed for the determination of the heat duty of the fired heater are displayed in Table 3

2.4. Cost estimation

In this study, the costs of the membrane and zeolite-based processes are sub-divided in process operation costs and investments costs. Process operation costs include consumption costs for i.e. the electrical energy, natural gas or cooling water. The investment costs, being fixed annual expenses [24], are assigned to the purchase and mounting of the processes operation units. Since the investment is exclusively financed through loans, it is composed of the interest payment and the principal repayment [25].

Costs related to labor are not taken into account in this assessment since their prediction cannot be made without large error margins. However, fewer shifts are needed for the continuously running membrane-based process than for the semi-batch zeolite-based process, indicating lower labor costs for the membrane-based process.

Table 4 displays a price list of various utilities, which are needed for the operational costs calculation of both processes. Since membranes have a limited lifetime of 4 years, the mean annual expenditure assigned to their purchase is included in the costs of the membrane-based process [8]. The same applies to the zeolite, which has an estimated lifetime of 2 years [8].

The major part of the electricity is used by compressors to pressurize CO₂ to its supercritical state or to recirculate or transport large air to the fired direct heater in case of the zeolite-based process. The electrical power consumption of compressors is determined using the adiabatic compressor power equation for high pressures (above 70 bar) [28], as described by:

$$W_i = \frac{1}{\varepsilon} \cdot P_{out} \cdot \dot{V}_{flow} \cdot \frac{k_i}{k_i - 1} \cdot \left(\left(\frac{P_{out}}{P_{in}} \right)^{\frac{k_i - 1}{k_i}} - 1 \right) \cdot \left(\frac{Z_{out} + Z_{in}}{2 \cdot Z_{out}} \right) \quad (15)$$

Table 4
Values used for the determination of the operational costs of both processes.

Parameter	Value	Reference
Selective skin layer (based on 1 μm thickness)	3 €/m ²	[est.]
Porous support	244 €/m ²	[26]
Lifetime membrane	4 year	[8]
Electrical energy	0.14 €/kWh	[27]
Cooling water	0.04 \$/m ³	[25]
Steam for heating (saturated at 8 bar, 170 °C)	0.006 \$/kg	[25]
Price of natural gas	0.035 €/kWh	[27]
Price of zeolite	3 €/kg	[8]
Lifetime zeolite	2 year	[8]
Energy demand for reactivation of Zeolite	11,880 kJ/kg _{H₂O}	[8]

P_{in} and P_{out} are the pressures at the compressor in- and outlet (Pa), \dot{V}_{flow} is the volume flow rate of the transported fluid at the compressor outlet (m³/s), k_i is the ratio of the specific heat capacities at constant pressure and constant volume and ε is the compressor efficiency, both being dimensionless (–). The compressor efficiency is considered to be 0.7 [25]. The required heat capacities are obtained from the official website of the National Institute of Standards and Technology (NIST) and averaged for the required pressure ranges [29]. The electrical power consumption of commercially available air driers is used [30].

The compressors used in both processes run throughout the year (8760 h/year). Only the compressor blowing air through the direct-fired heater is not in use during the cool-down phase of the zeolite, which makes up, according to Table 3, 25% of the time.

The starting point for the determination of the investment costs is the estimation of the total costs related to the purchase and implementation of the considered units (incl. piping and instrumentation) into the process. The investment costs (IC) of the process units are determined through the widely used method developed by Guthrie [24]:

$$IC = BC \cdot UF \cdot (MPF + MF - 1) \quad (16)$$

where BC are the purchase costs of the basic version of the process unit for a particular year given in €, UF is the update factor (–) taking the price increase of the unit through inflation from the particular year to presence into account, MPF is the materials and pressure correction factor which accounts for additional material and design costs of the process unit beyond its basic configuration (–) and MF is the module factor (–) which takes the costs of piping instruments, labor during mounting and accessories into account.

The basic costs for the considered heat exchangers and the direct-fired heater are obtained from Peters et al. [25] whereas the basic costs for the used compressors, vessels, and columns are obtained from Biegler et al. [24]. The basic cost obtained from Peters et al. [25] and Biegler et al. [24] are dated back to the years 1990 and 1969, respectively. The basic costs of vessels are used for the housing of the membrane unit, the zeolite columns, and the extraction unit. However, these costs are increased by 100% for the housing of the membrane unit and 20% for the extraction unit and the zeolite columns due to the higher complexity (i.e., stack frame, distribution equipment, fixtures, trays, sensors) compared to a simple vessel.

To determine the annual expenses related to the investment, the total investment costs are multiplied by the so-called capital-recovery factor CRF which is represented by:

$$CRF = \frac{(1 + i)^n \cdot i}{((1 + i)^n - 1)} \quad (17)$$

where i is the interest rate (%), and n is the loan duration (years).

Table 5 lists the relevant parameters used for the determination of the costs of the use of the capital to purchase the equipment.

Table 5
Relevant parameters needed to determine investment costs.

Costs parameters	Value	Reference
Interest rate of the loan	8.0%	[est.]
Duration of the loan	10 year	[est.]
Exchange rate USD in EUR	1.14 \$/€	[31]
Capital-recovery factor	0.15356	[calc. ^a]
Annual operation hours	8760 h/yr	[32]
Chemical engineering plant cost index (Feb. 2017)	558.3	[33]

^a calc. = calculated

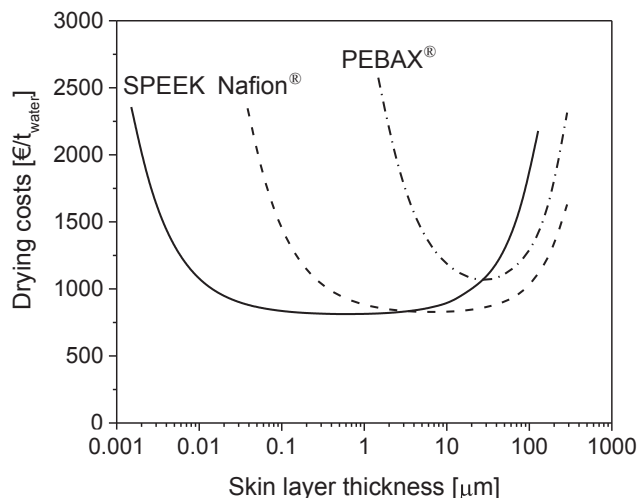


Fig. 4. Total (normalized) drying costs using either a SPEEK, Nafion® 117 or PEBAX® 1074 selective membrane layer as a function of the skin layer thickness, for a dehydration rate (process scale) of 100 kg water per hour at 45 °C.

3. Results and discussion

3.1. Effect of skin layer thickness

Our previous study [9] suggests that for the membrane-based process there is an ideal skin-layer thickness at which the drying costs are minimal. Fig. 4 displays the effect of the skin layer thickness on the total drying costs normalized for the amount of water removed at 45 °C for SPEEK, Nafion® 117 and PEBAX® 1074.

All three membrane types show an optimum in skin layer thickness, i.e., a range at which the total drying costs are minimal. Despite the similarity, the membranes differ in the position of this minimum as well as the range over which this minimum extends. Fig. 5 explains in more detail the behavior observed, i.e., the shape of the curves, by showing the same SPEEK data but in addition the costs for CO₂ refill and the membrane unit.

For SPEEK the total drying costs show a minimum for a skin layer thickness ranging from approximately 0.1 to 10 μm. At a thickness < 0.1 μm, costs increase because the permeability of the SPEEK layer to CO₂ becomes too high (due to the low thickness of the layer), resulting in rising costs for CO₂ refill. At a thickness > 10 μm, costs increase because the permeability towards H₂O becomes too low, resulting in larger required membrane surface areas. From 10 μm downward, membrane unit costs remain unchanged because at these skin layer thicknesses concentration polarization effects dominate H₂O transport.

Compared to SPEEK, the minima of Nafion® 117 and PEBAX® 1074 have shifted to larger skin layer thicknesses, reflecting that PEBAX demonstrates the lowest H₂O/CO₂ selectivity (notably due to a high CO₂ permeability) whereas Nafion shows the highest H₂O permeability combined with a moderate permeability towards CO₂.

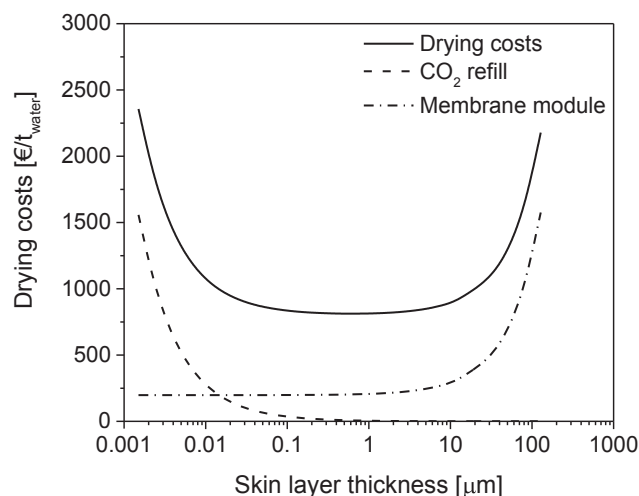


Fig. 5. Total (normalized) drying costs using SPEEK as a function of the skin layer thickness, for a dehydration rate (process scale) of 100 kg water per hour at 45 °C. Also shown are the costs for CO₂ refill and the membrane unit.

Based on the three examined skin layer materials discussed in Fig. 4, SPEEK is considered the material of choice, since it shows with 813 €/t_{water} the lowest drying costs compared to values of 828 and 1063 €/t_{water} for Nafion® 117 and PEBAX® 1074 respectively. In addition, the costs of SPEEK remain at this minimum even at skin layers as thin as 0.1 μm, leading to less material required and thus cost savings.

3.2. Process configuration

The feed boundary layer is the dominant parameter in the H₂O flux across the membrane [9]. As such, this mass transfer resistance should be taken into account as well, in addition to those related to the membrane itself. Fig. 6 exemplifies this argument and shows the calculated total membrane area required to permeate 100 kg of water per hour taking into account the individual effect of the mass transfer resistance of the skin layer, the feed boundary layer, the permeate boundary layer and the porous support.

As expected, the porous support (low resistance) and the permeate boundary layer hardly affect the required membrane area. In contrast, ignoring the feed boundary layer resistance lowers the required

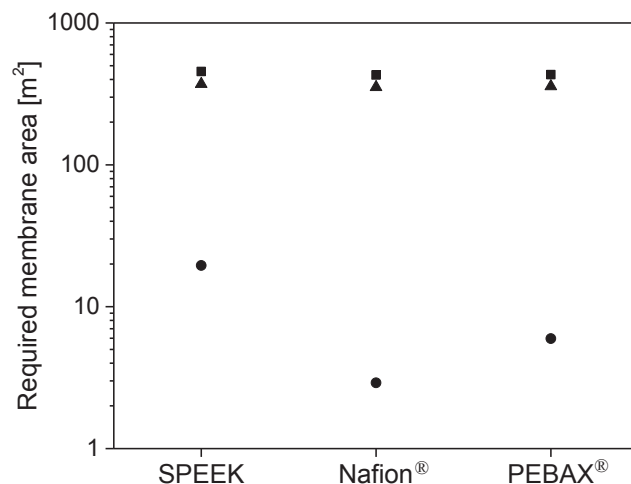


Fig. 6. Calculated total membrane area required to permeate 100 kg H₂O per hour at 45 °C for SPEEK, Nafion® 117 and PEBAX® 1074. Calculations include either (●) solely the skin layer; (▲) the feed boundary and skin layer or (■) feed and permeate boundary, support and skin layer.

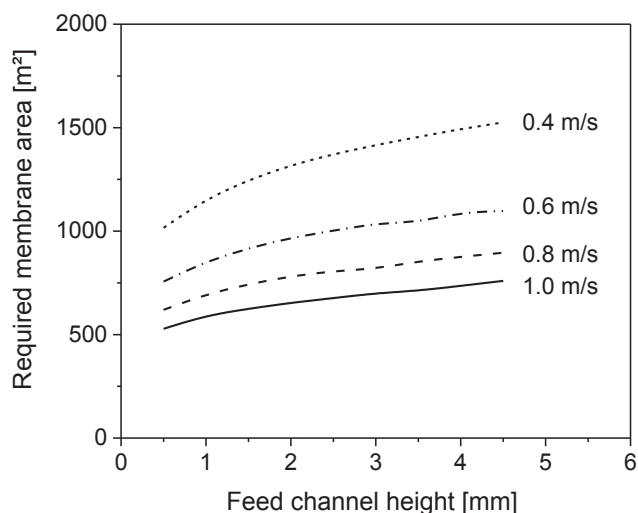


Fig. 7. Required membrane area to permeate 100 kg water per hour as a function of the feed channel height for various cross-flow velocities for SPEEK membranes at 45 °C.

membrane area by more than a factor of 40 (SPEEK) to 150 (Nafion® 117).

Given the overwhelming impact of feed boundary resistance on the required membrane area and the dominance of the required membrane area on membrane unit and CO₂ refill costs, we investigate strategies to lower this resistance by altering fluid dynamics within the membrane unit. Note that, a reduction of the required membrane area is accompanied by a reduction of the membrane unit and CO₂ refill costs.

Fig. 7 displays the required total membrane area in relation to the feed channel height, at different cross-flow velocities.

One method to reduce the feed boundary layer resistance is by increasing the cross-flow velocity, as experimentally observed by Metz et al. [15]. This way of invoking turbulent conditions leads to a steeper cross-flow velocity profile and thus to a thickness reduction of the boundary layer [34], in which H₂O is transported limited by diffusion. Decreasing the feed channel height while maintaining an average cross-flow velocity leads as well to a steeper cross-flow velocity profile and thus to a reduced fluid boundary layer thickness [34]. This together with an increase of the cross-flow velocity will lead to increased pressure drop, as is evident from Eq. (10). From here on, the feed channel height and cross-flow velocity adopt values of 0.8 mm and 1 m/s, respectively.

Another way of reducing the feed boundary layer resistance and thus the required membrane area is by altering the temperature and feed pressure. As argued in the previous study [9], high pressures and low temperatures, as present in the default membrane configuration (Fig. 2), lead to a more dominant feed boundary layer resistance, hampering the H₂O transport. Other process parameters, such as H₂O transport driving force, may be affected by pressure and temperature as well. Fig. 8 shows the required total membrane surface area in relation to the feed chamber pressure and temperature.

The general tendency is that high dehydration temperatures and low feed pressures result in a reduction of the required membrane surface area, an effect much more pronounced at lower temperature. At an operational pressure of 130 bar, increasing the temperature from 45 to 65 °C reduces the required membrane surface area from 455 m² to 127 m². Apart from the already argued effect on the feed boundary layer thickness, another reason for this drastic reduction in required membrane surface area can be found in the rise of the water fugacity coefficient from 0.143 (at 45 °C; 130 bar) to 0.278 (65 °C; 130 bar), resulting in a doubling of the water fugacity in the feed (see equation (4)) and thus to a rise of the driving force for water transport (water fugacity coefficient determined using the model of Spycher et al. [5]).

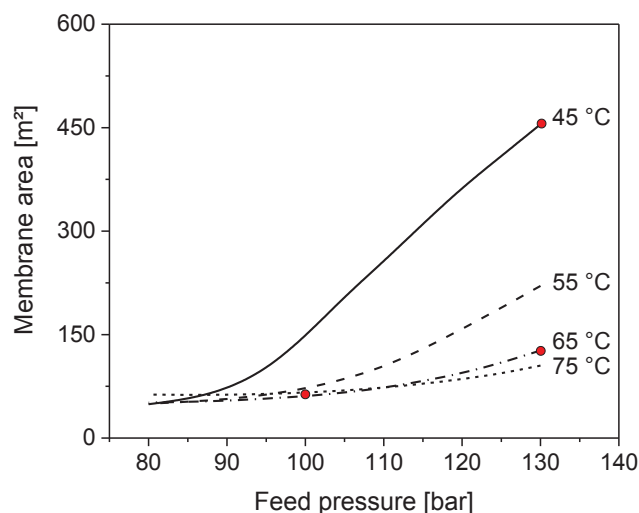


Fig. 8. Required membrane surface area to permeate 100 kg of water per hour depicted as a function of the feed pressure and the dehydration temperature. Feed channel height and cross-flow velocity are 0.8 mm and 1 m/s, respectively. The red dots indicate three feed conditions within the membrane unit which corresponding dehydration processes are economically assessed. (For interpretation of the references to colour in this figure legend, the reader is referred to the web version of this article.)

An additional reason for the strong reduction in the required membrane surface area may be an improved water diffusion through the feed boundary layer, due to a reduced CO₂ fluid density [9]. Even though the reduction of the membrane surface area to 127 m² results in a drop of the costs for CO₂ refill and the membrane unit, energy consumption will go up due to the heat exchangers needed to pre-heat and cool-down the scCO₂ before and after the membrane unit. A process based on this principle is displayed in Fig. 9. Noteworthy, an increase of the dehydration temperature to 75 °C will not significantly further reduce the required membrane surface area, but it will increase the costs for heat exchangers as well as the risk of material failure.

As indicated in Fig. 8, a further reduction of the required membrane area down to 61 m² can be achieved by reducing, at 65 °C, the feed pressure down to 100 bar. Here costs for the CO₂ refill and the membrane unit are further reduced. However, costs assigned to the

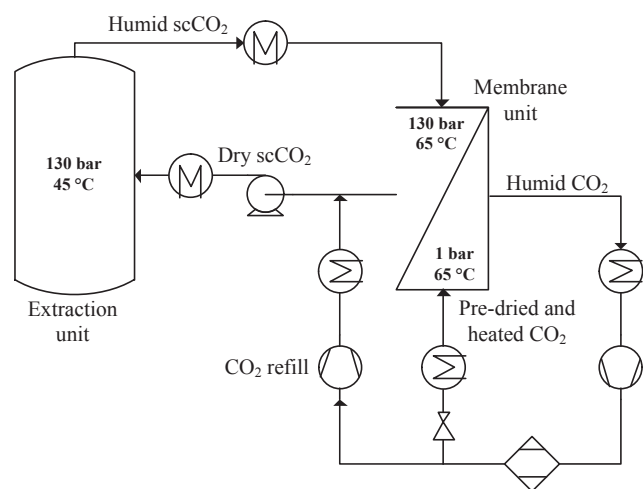


Fig. 9. Schematic depiction of a food dehydration process using scCO₂ as the water-extraction agent (left unit) and a membrane unit to dehydrate (regenerate) scCO₂. The pre-heated scCO₂ requires a lower membrane area thus reduced costs for the membrane unit and the CO₂ refill, however, additional costs for the purchase and investment of the additional heat exchangers.

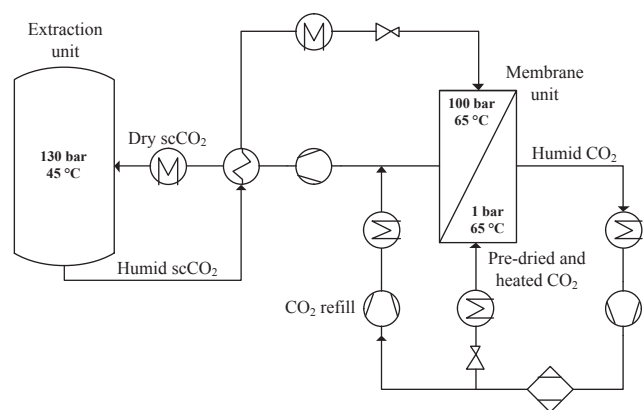


Fig. 10. Schematic depiction of a food dehydration process using scCO_2 as the water-extraction agent (left unit) and a membrane unit to dehydrate (regenerate) scCO_2 . The pre-heated and depressurized scCO_2 requires the smallest membrane area thus reduced costs for the membrane unit and the CO_2 refill, however, additional costs for the purchase and investment of the additional heat exchangers and the compressor.

circulation of the scCO_2 increase, due to the need of a costly compressor to pressurize the scCO_2 steam back to 130 bar after exiting the membrane unit, accordingly the process scheme of Fig. 10.

Fig. 11 compares the total drying costs as function of process scale of all three membrane based configurations, as displayed in Figs. 2, 9, and 10, with the zeolite-based benchmark process of Fig. 1.

Fig. 11 gives rise to several conclusions. Firstly, all processes show a decrease in drying costs with increased process scale with, at larger scale, the drying costs become essentially insensitive to process scale. This effect, where the specific costs are reduced with rising process scale, is generally referred to as economy of scale [35]. Secondly, independent of scale, all membrane-based processes show lower drying costs than the zeolite-based process. Thirdly, the process displayed in Fig. 2 is the least cost-effective membrane-based configuration, even though no heat exchangers nor compressors are implemented on the high-pressure side. The costs assigned to the membrane unit and CO_2 refill dominate the total drying costs. Lastly, Fig. 9 outlines the most cost-effective configuration, operating at a feed pressure and temperature of 130 bar and 65 °C. The cost-effectiveness of the latter configuration is the result of its small required membrane area, being, according to Fig. 8, one third of the size of the configuration operating at

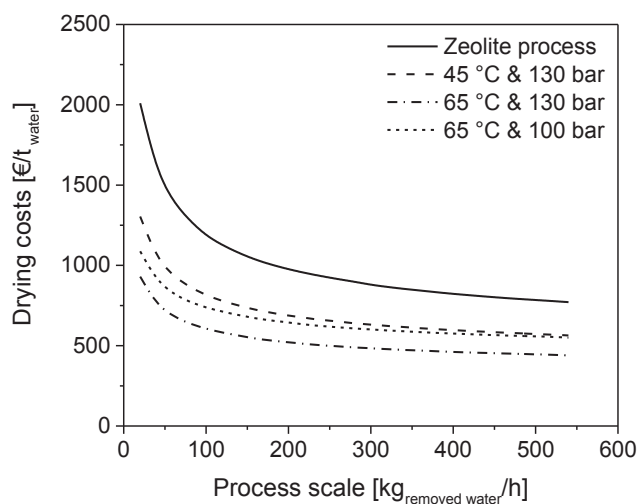


Fig. 11. Comparison of the drying costs of various membrane-based processes with the current benchmark process based on zeolite. This is done for various process scales.

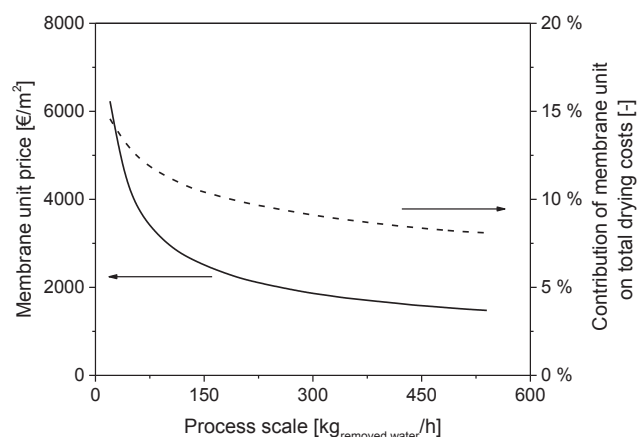


Fig. 12. The area specific costs of the membrane unit and its contribution to the total process costs as a function of the process scale. Feed pressure and process temperature are 130 bar and 65 °C, respectively.

130 bar and 45 °C and the absence of any compression and depressurization step in its feed cycle. Such pressure changes in the feed cycle, as occur in the configuration operating at 100 bar and 65 °C, result in inflated drying costs. The drying costs assigned to this configuration are approximately half (48–57%) the costs of a zeolite-based process. In absolute terms, the drying costs corresponding to Fig. 9 are 756 and 446 € per ton removed water, for a pilot plant scale (40 kg/h) and industrial scale (500 kg/h), respectively.

3.3. Membrane unit & membrane material

Based on the configuration of Fig. 9, Fig. 12 displays the membrane unit costs and its contribution to the total drying costs as a function of process scale.

Compared to the configuration and operational conditions displayed in Fig. 2 (130 bar, 45 °C), the contribution of membrane unit costs are reduced from 25 to 10%. With a membrane unit price of 4480 €/m² for pilot plant scale (40 kg/h) to 1520 €/m² for large industrial scale (500 kg/h), prices are considerably higher than those for membrane units operating near ambient pressures, 200 €/m² [36]. The combination of a costly housing for the membrane unit, built to withstand large operation pressures, and a low area to volume ratio of the membrane unit, is the primary cause for the inflated area specific costs. The low area to volume ratio of the current design, 65 m²/m³ compared to 100–300 m²/m³ of typical flat sheet units [37], is the result of wide sweep gas channels (3 mm) needed to pass sufficient sweep gas, without creating too high-pressure drops. A vast quantity of sweep gas is needed to remove a sufficient amount of permeate water without becoming too humid, thereby impairing the driving force too much.

Fig. 13 displays the fictional membrane unit price at which the drying costs of the membrane-based process would comprise 60%, 80% and 100% of those of the zeolite process.

Using Fig. 13 in practice, it becomes possible to determine the upper price limit for the purchase or development and construction of a membrane unit. To comprise 60% of zeolites drying costs, the price of the membrane unit has to triple at pilot plant scale (40 kg/h) and double at industrial scale (500 kg/h). This shows that the membrane-based process will continue to be cost efficient even with considerably higher membrane unit prices.

Not only the membrane unit price might be different in practice but also the considered permeability values of SPEEK obtained at 30 °C and near ambient pressures (feed pressure of 2.5 bar [14]) will most likely rise when applied at 130 bar and 65 °C. Bos et al. [38], who examined eleven glassy polymeric membranes (i.e., polysulfone, polyetherimide) observed a gradually progressing increase in CO_2 permeability while

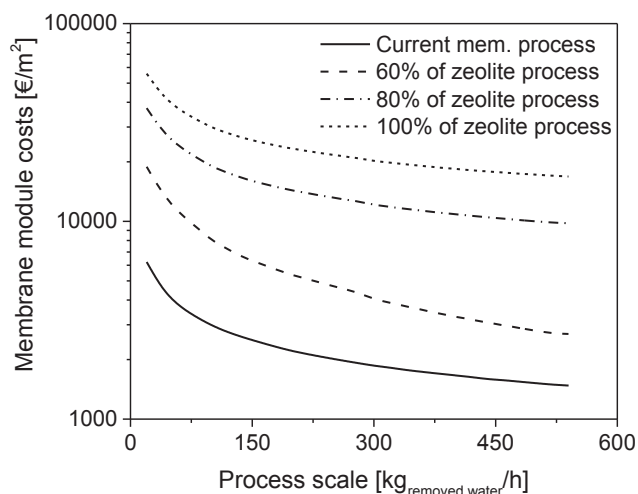


Fig. 13. The area specific costs of the membrane unit as a function of the process scale and the cost relation to the zeolite-based process. Feed pressure and process temperature are 130 bar and 65 °C, respectively.

exceeding a specific pressure, called plasticization pressure, which ranges between 10 and 34 bar, thus far below the applied 130 bar of the dehydration process. This sudden change was assigned to a transition of the polymer state from glassy to rubbery. This transition leads to increased mobilization of the polymer chains and thus to increased penetrant diffusion. Penetrant diffusion is also promoted by higher temperatures [14]. Fig. 14(a) and (b) display the sensitivity of the drying costs on the variation of H₂O and CO₂ permeability in a SPEEK based system.

The drying costs displayed in Fig. 14(a) and (b) decrease with decreasing CO₂ permeability and with increasing H₂O permeability. This is in accordance to the findings of Fig. 5 where a more CO₂ permeable skin layer results in inflated CO₂ refill and thus drying costs and a less H₂O permeable skin layer leads to larger membrane areas and increased drying costs.

The drying costs are insensitive for H₂O permeabilities of 10,000 Barrer or higher and CO₂ permeabilities of 10 Barrer or lower. For skin layer materials lying within these boundaries, the drying costs maintain close to optimum, thus making them suitable alternatives to the current material of choice, namely SPEEK. However, the CO₂ permeability of SPEEK, being 0.11 Barrer (at 30 °C and 2.5 bar) might increase significantly when applied at the high feed pressure and temperature. Nafion® 117 lies within these boundaries whereas PEBAX® 1074 exceeds the boundary set by the CO₂ permeability. For a PEBAX® 1074 based system costs related to CO₂ refill would dominate the total drying costs up to an extent at which the process becomes more cost-intensive

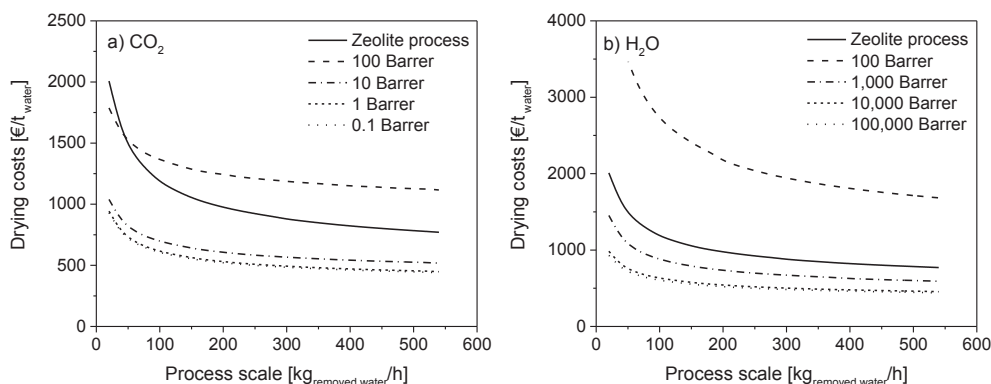


Fig. 14. Drying costs as a function of the process scale and (a) CO₂ permeability for (b) H₂O permeability. The permeabilities of SPEEK, being 61,000 for H₂O and 0.11 Barrer for CO₂, are the basis for the non-altered permeability values. Feed pressure and process temperature are 130 bar and 65 °C, respectively.

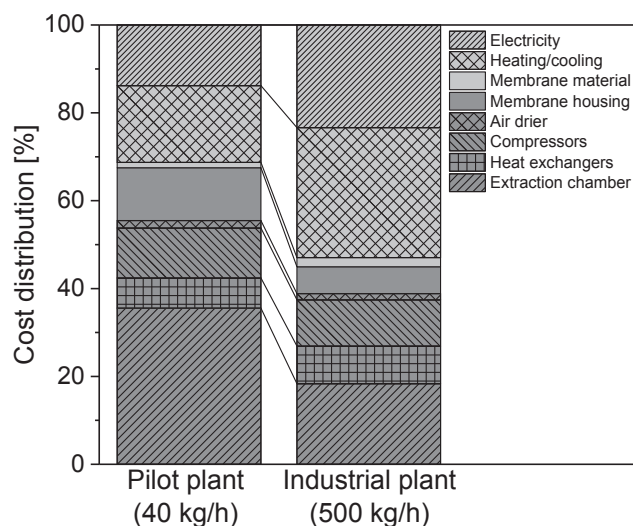


Fig. 15. Cost distribution of the membrane-based process (configuration 130 bar; 65 °C). Light grey bar sections indicate operational costs, dark grey sections investment costs.

than the zeolite process.

Fig. 15 summarizes our findings and delineates the relative costs involved in the scCO₂ drying process using a SPEEK-based membrane with a skin layer thickness of 1 μm, operating at feed chamber pressure of 130 bar and temperature 65 °C, for two process scales, 40 and 500 kg/h. Investment and operational costs are represented by dark and light grey bar sections, respectively. Irrespective the scale, costs of the extraction chamber, i.e., steam and electricity costs for heating and cooling, dominate the picture. Nevertheless, even though total membrane costs (membrane material + housing) contribute far less, its share in total costs still mounts up to 10% and even more at pilot plant scale. Lohaus et al. [8], concluded that, based on their calculations, membrane costs can be considered negligible compared to the other costs. The discrepancy in outcome reflects the differences in analysis as the present study does include boundary layer effects and costs related to the membrane housing, not only those for the membrane material.

4. Conclusions

This study showed that there is an ideal skin-layer thickness at which the drying costs of scCO₂ reach a minimum. Too thin skin layers result in inflated CO₂ refill costs due to increased CO₂ permeation towards the permeate side, whereas a too thick layer, leads to lower H₂O permeation thus to larger membrane areas and inflated membrane unit costs. Based on a selection of different membrane materials, SPEEK was

considered the material of choice since it leads to the lowest drying costs over the broadest range of skin layer thicknesses. The consideration of concentration polarization effects in the feed boundary layer results in membrane areas which are 150 larger than when omitting these effects. To encounter these H₂O flux hampering effects fluid dynamics have to be altered, such as reducing the feed chamber height, increasing crossflow velocity or choosing feed pressures and dehydration temperatures at which the Reynolds number is maximal. The choice of feed pressure and dehydration temperature has a significant impact on the required membrane area. An increase of the dehydration temperature from 45 °C to 65 °C, while keeping the feed pressure at 130 bar, reduces the required membrane area to remove 100 kg of water per hour, from 455 m² down to 127 m². Therefore, three process configurations differing in their feed pressure and dehydration temperature and the zeolite-based benchmark process were compared regarding their drying costs, for various scales ranging from water removal rate from 40 kg/h to above 500 kg/h. The configuration having 130 bar and 65 °C as feed pressure and dehydration temperature proved to be the most cost-efficient comprising half the drying costs of the benchmark process based on zeolite and was therefore considered the process of choice. The membrane unit considered in this configuration comprises only 10% of the total drying costs but shows with 4480 €/m² (pilot plant scale) and 1520 €/m² (industrial scale) significantly high area specific costs. Reasons are found in the costly high-pressure membrane unit housing and the low area to volume ratio of the membrane unit.

The drying costs are insensitive for H₂O permeabilities of 10,000 Barrer or higher and CO₂ permeabilities of 10 Barrer or lower. Skin layer materials lying within these boundaries are considered potential alternatives to SPEEK being the current material of choice for the dehydration of supercritical CO₂.

Acknowledgments

This work was performed in the cooperation framework of Wetsus, European Centre of Excellence for Sustainable Water Technology (www.wetsus.nl). Wetsus is co-funded by the Dutch Ministry of Economic Affairs and Ministry of Infrastructure and Environment, the European Union Regional Development Fund, the Province of Fryslân, and the Northern Netherlands Provinces. The authors like to thank the participants of the research theme Dehydration (Feyecon, Avebe) for the fruitful discussions and their financial support.

References

- [1] A. Clifford, *Fundamentals of Supercritical Fluids*, Oxford University Press, New York, USA, 1998.
- [2] S. Khaloufi, C. Almeida-Rivera, P. Bongers, Supercritical-CO₂ drying of foodstuffs in packed beds: experimental validation of a mathematical model and sensitive analysis, *J. Food Eng.* 96 (1) (2010) 141–150.
- [3] Z.K. Brown, P.J. Fryer, I.T. Norton, S. Bakalis, R.H. Bridson, Drying of foods using supercritical carbon dioxide — investigations with carrot, *Innov. Food Sci. Emerg. Technol.* 9 (3) (Jul. 2008) 280–289.
- [4] R. Smith Jr, H. Inomata, M. Kanno, K. Arai, Energy analysis of supercritical carbon dioxide extraction processes, *J. Supercrit. Fluids* 15 (2) (1999) 145–156.
- [5] N. Spycher, K. Pruess, J. Ennis-King, CO₂-H₂O mixtures in the geological sequestration of CO₂. I. Assessment and calculation of mutual solubilities from 12 to 100 °C and up to 600 bar, *Geochim. Cosmochim. Acta* 67 (16) (2003) 3015–3031.
- [6] A. Birtigh, J. Stoldt, G. Brunner, New method for supercritical fluid regeneration, *J. Supercrit. Fluids* 8 (2) (1995) 162–166.
- [7] G. Dilip, D. Shantanu, B. Debasis, *Innovation in Healthy and Functional Foods*, CRC Press, Boca Raton, FL, USA, 2016.
- [8] T. Lohaus, M. Scholz, B.T. Koziara, N.E. Benes, M. Wessling, Drying of supercritical carbon dioxide with membrane processes, *J. Supercrit. Fluids* 98 (2015) 137–146.
- [9] A. Shamu, H. Miedema, S.J. Metz, Z. Borneman, K. Nijmeijer, Mass transfer studies on the dehydration of supercritical carbon dioxide using dense polymeric membranes, *Sep. Purif. Technol.* 209 (July 2018) (2019) 229–237.
- [10] F. Kaymak-Ertekin, A. Gedik, Sorption isotherms and isosteric heat of sorption for grapes, apricots, apples and potatoes, *LWT - Food Sci. Technol.* 37 (4) (2004) 429–438.
- [11] M. E. Dauthy, *Fruit and vegetable processing*, No.117, Food and Agriculture Organization of the United Nations, Rome, 1995.
- [12] J.J. McKetta Jr., *Encyclopedia of Chemical Processing and Design: Volume 59 - Trays versus Packing in Separator Design*, CRC Press, New York, USA, 1997.
- [13] M. Dingemans, et al., Mass transfer characteristics for VOC permeation through flat sheet porous and composite membranes: the impact of the different membrane layers on the overall membrane resistance, *J. Memb. Sci.* 322 (1) (2008) 234–242.
- [14] H. Sijbesma, K. Nijmeijer, R. van Marwijk, R. Heijboer, J. Potreck, M. Wessling, Flue gas dehydration using polymer membranes, *J. Memb. Sci.* 313 (1–2) (Apr. 2008) 263–276.
- [15] S.J. Metz, W.J.C. Van De Ven, J. Potreck, M.H.V. Mulder, M. Wessling, Transport of water vapor and inert gas mixtures through highly selective and highly permeable polymer membranes, *J. Memb. Sci.* 251 (1–2) (2005) 29–41.
- [16] S.H. Choi, M.S. Qahtani, E.A. Qasem, Multilayer thin-film composite membranes for helium enrichment, *J. Memb. Sci.* 553 (2018) 180–188.
- [17] H. Lin, et al., Dehydration of natural gas using membranes. Part I: Composite membranes, *J. Memb. Sci.* 413–414 (2012) 70–81.
- [18] H.L.M. Lelieveld, J. Holah, D. Napper, *Hygiene in Food Processing: Principles and Practice*, second ed., Woodhead Publishing Limited, Cambridge, UK, 2014.
- [19] R. Perry, D. Green, J. Maloney, *Perry's chemical engineers' handbook*, no. 7th, 1997.
- [20] D. Newnan, Surface roughness coefficient, in: *Civil Engineering: License Review*, Kaplan AEC Engineering, Chicago, IL, USA, 2004, p. 747.
- [21] E. Gabrus, J. Nastaj, P. Tabero, T. Aleksandrak, Experimental studies on 3A and 4A zeolite molecular sieves regeneration in TSA process: aliphatic alcohols dewatering-water desorption, *Chem. Eng. J.* 259 (2015) 232–242.
- [22] Aldrich-Sigma, *Molecular Sieves - Technical Information Bulletin*, 2017. Available: < <http://www.sigmaaldrich.com/chemistry/chemical-synthesis/learning-center/technical-bulletins/al-1430/molecular-sieves.html> > (accessed: 02-Oct-2017).
- [23] S. Ramaswamy, H.-J. Huang, B.V. Ramarao, *Separation and Purification Technologies in Biorefineries*, John Wiley & Sons Ltd, 2013.
- [24] L. Biegler, I.E. Grossmann, *Systematic Methods of Chemical Process Engineering: Equipment Sizing and Costing*, first ed., Prentice Hall, New Jersey, USA, 1997.
- [25] M.S. Peters, K.D. Timmerhaus, R.E. West, *Plant Design and Economics for Chemical Engineers*, fourth ed., McGraw-Hill Inc, Singapore, 1991.
- [26] Sterlitech Corporation, *Pricelist of Nylon membranes*, 2017. Available: < <https://www.sterlitech.com/nylon-membranes.html> > . (accessed: 27-Jun-2017).
- [27] Eurostat, *Energy price statistics*, 2016. Available: < http://ec.europa.eu/eurostat/statistics-explained/index.php/Energy_price_statistics > (accessed: 27-Jun-2016).
- [28] N. Petchers, *Combined Heating, Cooling & Power Handbook: Technologies & Applications: An Integrated Approach to Energy Resource Optimization*, The Fairmont Press, Liburn, GA, USA, 2003.
- [29] *Thermophysical Properties of Fluid Systems - NIST: National Institute of Standards and Technology*, 2016. Available: < <http://webbook.nist.gov/chemistry/fluid/> > (accessed: 05-Apr-2017).
- [30] Kaeser Compressors Inc., *Refrigerated Air Dryers*, Available: < http://us.kaeser.com/Products_and_Solutions/Compressed-air-treatment/Drying/refrigerated-air-dryers/refrigerated-compressed-air-dryer.asp#0 > (accessed: 27-Jun-2017).
- [31] L.P. Bloomberg, *EURUSD Spot Exchange Rate*, 2015, Available: < <http://www.bloomberg.com/quote/EURUSD:CUR> > (accessed: 13-Oct-2015).
- [32] S. Skogestad, *Chemical and Energy Process Engineering*, CRC Press, Boca Raton, FL, USA, 2008.
- [33] *Chemical Engineering, Chemical engineering plant cost index of February 2017*, 2017, Available: < <http://www.chemengonline.com> > (accessed: 20-Jul-2018).
- [34] H. Schlichting, K. Gersten, *Boundary-Layer Theory*, 8th Revise, Springer-Verlag, Berlin Heidelberg, Berlin, Germany, 2003.
- [35] D.R. Seider, W.D. Seader, J.D. Lewin, *Economy of scale and the six-tenths factor, Product and Process Design Principles – Synthesis, Analysis, and Evaluation*, John Wiley & Sons Ltd, 2003, p. 820.
- [36] R.W. Baker, *Membrane Technology and Applications*, 2004.
- [37] S. Judd, B. Jefferson, *Table 2.5 Membrane configurations*, in: *Membranes for Industrial Wastewater Recovery and Re-use*, Elsevier Ltd, Oxford, UK, 2003, p. 291.
- [38] A. Bos, I.G.M. Pünt, M. Wessling, H. Strathmann, CO₂-induced plasticization phenomena in glassy polymers, *J. Memb. Sci.* 155 (1) (1999) 67–78.